Multi-interaction mean-field renormalization group

C. N. Likos[1] and A. Maritan[2]
[1]*Dipartimento di Fisica Teorica, Università di Trieste, Strada Costiera 11, I-34014 Grignano, Trieste, Italy*
[2]*Istituto Nazionale di Fisica della Materia (INFM), Scuola Internazionale Superiore di Studi Avanzati and Istituto Nazionale di Fisica Nucleare, Sezione di Trieste, via Beirut 2-4, I-34013 Trieste, Italy*
(Received 27 September 1995)

We present an extension of the previously proposed mean-field renormalization method to model Hamiltonians that are characterized by more than just one type of interaction. The method rests on scaling assumptions about the magnetization of different sublattices of the given lattice and it generates as many flow equations as coupling constants without arbitrary truncations on the renormalized Hamiltonian. We obtain good results for the test case of Ising systems with an additional second-neighbor coupling in two and three dimensions. An application of the method is also done to a morphological model of interacting surfaces introduced recently by Likos, Mecke, and Wagner [J. Chem. Phys. **102**, 9350 (1995)].

PACS number(s): 64.60.Ak, 64.60.Fr, 05.70.Jk

I. INTRODUCTION

One of the simplest techniques for deriving renormalization group recursions is the so-called mean-field renormalization group (MFRG) of Indekeu, Maritan, and Stella [1]. The MFRG has proven to be an efficient method for the calculation of critical couplings and exponents of a wide variety of lattice models. The range of applications of the MFRG extends beyond the study of bulk critical phenomena in classical systems, to include quantum models and surface criticalities; moreover, extensions of the MFRG ideas to dynamical critical phenomena have also been presented [2,3].

The most appealing features of the MFRG are its simplicity and its direct connection with the classical mean-field ideas; whereas mean-field theory is a simple approach to the study of the phase behavior of various models in statistical mechanics, its most serious drawback is that it predicts the wrong (classical) critical exponents. The MFRG offers a way to remedy this deficiency while maintaining some basic notions from the mean-field approximation (e.g., the effective field).

We shall now summarize the main ideas of the original MFRG. To illustrate the method, let us consider the nearest-neighbor Ising model which is described by the Hamiltonian

$$H \equiv -\beta\mathcal{H} = h\sum_i s_i + J\sum_{\langle ij\rangle} s_i s_j \ , \tag{1.1}$$

where the second sum is carried over nearest-neighbor sites on a given lattice of dimension d. Consider now two clusters of interacting spins, containing N and N' sites, with $N' < N$. Suppose that the surrounding spins of these clusters are fixed at the values b ($|b| \le 1$) for the larger cluster and b' ($|b'| \le 1$) for the small one, and evaluate the magnetizations per site for both clusters, m and m', respectively. Clearly, m and m' depend on the coupling constant J, the magnetic field h, and the boundary values b and b'. Setting $m(J,h,b)=b$ or $m'(J,h,b')=b'$, we would obtain two different types of mean-field equations, which could then be solved self-consistently, and the criticality would be identified with the "bifurcation point" of either of the two equations for $h=0$ (each of the two equations yields a different approximate value J_c for the critical coupling, of course.) However, this approach leads to classical critical behavior. Instead, in the MFRG one uses the two cluster magnetizations to define a *mapping* $(J,h,b)\rightarrow(J',h',b')$ by requiring

$$m'(J',h',b') = s^{d-y_h} m(J,h,b) \tag{1.2}$$

together with

$$b' = s^{d-y_h} b \tag{1.3}$$

to hold to leading orders in h and b. In Eqs. (1.2) and (1.3) above, the rescaling factor s is defined as

$$s = (N/N')^{1/d} \ . \tag{1.4}$$

Setting $h=h'=0$, expanding both sides of (1.2) to linear order in b and b', and using (1.3) we obtain the RG flows for the coupling constant in the form

$$\left.\frac{\partial m'(J',h',b')}{\partial b'}\right|_{h'=0,b'=0} = \left.\frac{\partial m(J,h,b)}{\partial b}\right|_{h=0,b=0} \ . \tag{1.5}$$

Once the fixed points J_* of the iteration have been found from (1.5) the thermal and magnetic exponents y_t and y_h are determined through the relations

$$y_t = \frac{\ln\lambda_t}{\ln s} \ , \tag{1.6}$$

where

$$\lambda_t = \left[\left[\frac{\partial^2 m(J,h,b)}{\partial b\,\partial J}\right]\left[\frac{\partial^2 m'(J',h',b')}{\partial b'\partial J'}\right]^{-1}\right]\Bigg|_{J=J'=J_*,h=h'=0,b=b'=0} \tag{1.7}$$

and

$$\left.\frac{\partial m'(J',h',b')}{\partial h'}\right|_{J'=J_*,h'=0,b'=0} = s^{d-2y_h}\left.\frac{\partial m(J,h,b)}{\partial h}\right|_{J=J_*,h=0,b=0} . \tag{1.8}$$

As a rule, the MFRG yields better estimates for the critical coupling $J_c \equiv J_*$ than it does for the critical exponents. However, the latter can also be significantly improved in a number of ways. Slotte [4] has shown that a redefinition of the rescaling factor s leads to better values for the thermal exponent than the "naive" definition of s, Eq. (1.4) above. On the other hand, Indekeu, Maritan, and Stella [5] have succeeded in improving the MFRG critical exponents in a more systematic way, by considering three clusters and introducing an additional surface critical exponent y_{h_s}; this approach has led to a unified approach to bulk, surface, and corner critical behavior (see also Ref. [2]).

The remaining of the paper is organized as follows. In Sec. II we motivate and present an extended version of the MFRG. In Sec. III we test our approach by applying it to the square, simple cubic and body-centered cubic Ising models with crossing bonds, obtaining very good results for the fixed points and the overall phase behavior of these models. In Sec. IV we then apply this RG scheme to a morphological Hamiltonian of interacting surfaces [6]. In Sec. V we summarize and conclude. Since the derivation of the RG flows for the morphological model is rather lengthy, we outline the main steps in the Appendix.

II. EXTENDED MFRG

Let us consider, to begin with, what happens if we want to renormalize, by means of the simple MFRG scheme, a Hamiltonian in which the even interaction part (i.e., excluding the magnetic field and having a remainder which is invariant under $s_i \to -s_i$) contains more than just one type of interaction and thus more than one coupling constant. Denoting by $\mathbf{J} \equiv (J_1, J_2, \ldots, J_\nu)$ the ν-dimensional coupling constant of the Hamiltonian, the MFRG which is based on the scaling of a *single* order parameter (the bulk magnetization) always leads to a *single* flow equation, namely, one of the form (1.5) with J and J' replaced by their multidimensional counterparts $\mathbf{J}$ and $\mathbf{J}'$, respectively. Clearly, in order to specify the flows one needs as many equations as coupling constants in the Hamiltonian, so this single equation is not sufficient. In the vast majority of MFRG applications to many-coupling Hamiltonians, this equation was used in the following sense: a "fixed-point requirement" of the form $\mathbf{J}=\mathbf{J}'$ was made, which led to an equation of the form $f(\mathbf{J})=0$, identified as the equation which defines the critical surface of the model. Although such an approach has been widely used [2], and gives qualitatively correct results, it has the obvious drawback that it yields infinitely many "fixed points" (each point on the critical surface is "fixed"), and thus detailed information on the critical exponents is lost in this scheme. Moreover, the approach serves only to define the critical surface *alone* and not to determine the way in which each of the individual couplings J_α, $\alpha = 1,2,\ldots,\nu$, flows in the presence of the others. Therefore, such an approach is useful only in the sense that it provides us with better estimates of the critical surface of a given model than the simple mean-field approximation, requiring roughly the same amount of computational effort; but it does not offer a means for the renormalization of the Hamiltonian. The problem of a single recursion relation also occurs in the phenomenological renormalization of Nightingale [7], a question that has led Barber [8], to the development of an approach similar in spirit to ours.

There have been a few attempts to go beyond the above limitations of the MFRG: de Oliveira and Sá Baretto [9] studied the two-parameter Hamiltonian of the Ashkin-Teller (AT) model [10] and identified *two* order parameters in the problem. Making scaling assumptions about the order parameters of small and large clusters, they were then able to obtain flow diagrams of the usual type, finding isolated fixed points, critical exponents, etc. However, the AT model is one in which *two* different types of spin variables exist on the lattice sites, and this makes the introduction of two types of "magnetization" natural in this model. An approach which has some similarities to ours was presented by Plascak [11] for the case of the two-dimensional Ising model with crossing bonds. This approach is based on the selection of appropriate pairs of order parameters, depending on the region of the parameter space considered. However, this method leads to some ambiguities in the flows along the axis of vanishing first-neighbor coupling [11]. On the other hand, as we show below, our approach is free of such ambiguities.

We first present the basic conditions to be satisfied for the implementation of the method, at present. The types of models on which our approach is applicable must satisfy the following requirements (the discussion of more general cases is postponed for the concluding section):

(i) the interaction part of the Hamiltonian must be even, and it must contain only two coupling constants, call them J and K;

(ii) the model must be defined on a bipartite lattice; and

(iii) there must be a region of the parameter space for which there are only two kinds of ground states, a ferromagnetic (FM) and an antiferromagnetic (AFM) one, separated by some borderline of stability.

Once these prerequisites are satisfied, the approach proceeds as follows. Consider, as in the original formulation, two clusters of N and N' sites with $N' < N$. (Hereafter, primed and unprimed quantities will refer to quantities pertaining to the small and large clusters, respectively.) The clusters *must* be chosen in such a way that the two different sublattices of the given bipartite lattice are mutually equivalent in both clusters. Denoting the two

sublattices by A and B and fixing the surrounding sublattice magnetizations to the values b'_1 (b_1) and b'_2 (b_2) on the A and B sublattices, respectively, we then obtain by the usual mean-field procedure expressions of the type $m'_{A(B)}(J',K',h',b'_1,b'_2)$ and $m_{A(B)}(J,K,h,b_1,b_2)$ for the sublattice magnetizations of the small and big clusters. A mapping $(J,K,h,b_1,b_2)\rightarrow(J',K',h',b'_1,b'_2)$ is now defined, in analogy with Eqs. (1.2) and (1.3), through the requirements

$$m'_A(J',K',h',b'_1,b'_2)=s^{d-y_h}m_A(J,K,h,b_1,b_2)\ , \tag{2.1}$$

and

$$b'_i=s^{d-y_h}b_i,\quad i=1,2\ . \tag{2.2}$$

Equation (2.2) simply expresses the intuitively appealing requirement that the boundary magnetizations scale in the same way as the bulk ones, as in the original MFRG [1]. We adopt the usual definition $s=(N/N')^{1/d}$ for the rescaling factor. Setting again $h=h'=0$, expanding both sides of (2.1) to linear order in $b'_{1,2}$ and $b_{1,2}$, and using (2.2), we arrive at the flow equations for the coupling constants:

$$\left.\frac{\partial m'_A(J',K',h',\mathbf{b}')}{\partial b'_1}\right|_{h'=0,\mathbf{b}'=0}=\left.\frac{\partial m_A(J,K,h,\mathbf{b})}{\partial b_1}\right|_{h=0,\mathbf{b}=0} \tag{2.3}$$

and

$$\left.\frac{\partial m'_A(J',K',h',\mathbf{b}')}{\partial b'_2}\right|_{h'=0,\mathbf{b}'=0}=\left.\frac{\partial m_A(J,K,h,\mathbf{b})}{\partial b_2}\right|_{h=0,\mathbf{b}=0}, \tag{2.4}$$

where we have used $\mathbf{b}'$ and $\mathbf{b}$ as a shorthand for (b'_1,b'_2) and (b_1,b_2). Due to the equivalence of the two sublattices, the individual subcluster magnetizations obey the symmetry $m_A(J,K,h,b_1,b_2)=m_B(J,K,h,b_2,b_1)$ and the same for the primed quantities; thus the flows obtained if we use the B-sublattice magnetizations to perform the mapping are identical to (2.3) and (2.4) above. Hence the method generates *exactly two* independent flow equations, which are necessary and sufficient for the renormalization of the two-parameter Hamiltonian.

After the fixed points $\mathbf{J}_*\equiv(J_*,K_*)$ of the flows have been found, the nonmagnetic eigenvalues $\lambda_{1,2}$ and the critical exponents $y_{1,2}=\ln\lambda_{1,2}/\ln s$, as well as the associated eigenvectors, are evaluated by the usual procedure of linearizing around $\mathbf{J}_*$. The remaining magnetic exponent is calculated through the relation

$$\left.\frac{\partial m'_A(\mathbf{J}',h',\mathbf{b}')}{\partial h'}\right|_{\mathbf{J}'=\mathbf{J}_*,h'=0,\mathbf{b}'=0}=s^{d-2y_h}\left.\frac{\partial m_A(\mathbf{J},h,\mathbf{b})}{\partial h}\right|_{\mathbf{J}=\mathbf{J}_*,h=0,\mathbf{b}=0}\ . \tag{2.5}$$

Once more, due to the symmetry between m_A and m_B mentioned above, it is irrelevant which of the two is used for the evaluation of y_h. For the same reason, we can also work with the total magnetizations $m'=m'_A+m'_B$ and $m=m_A+m_B$, and derive y_h from the scaling of the susceptibility $\chi=\partial m/\partial h$ through

$$\chi'=s^{d-2y_h}\chi\ , \tag{2.6}$$

which will be useful later. We also note that, although the feature of working in the neighborhood of $b'=b=0$ is appropriate to the study of second-order transitions, the flow equations presented above are capable of producing also low-temperature fixed points with the associated $y_h=d$ magnetic exponent which is the signature of a first-order phase change [12].

Having developed the theoretical framework for our approximate renormalization technique, we proceed in the following two sections with specific applications.

III. ISING MODEL WITH CROSSING BONDS

In this section we apply the extended MFRG (EMFRG) to the case of the Ising model with first- and second-neighbor interactions (Ising model with crossing bonds.) The Hamiltonian reads as

$$H\equiv-\beta\mathcal{H}=h\sum_i s_i+J\sum_{\langle ij\rangle}s_is_j+K\sum_{\langle\langle ij\rangle\rangle}s_is_j\ , \tag{3.1}$$

where the second sum is carried over nearest sites and the third over next nearest sites. The model satisfies requirement (i) of Sec. II; in order to meet the requirement of a bipartite lattice, we must restrict our choices: in two dimensions, we will consider the square (sq) lattice, which can be split into two square sublattices. Moreover, the model on the square lattice has three types of ground states (for $h=0$): a doubly degenerate ferromagnetic one in the region $\{J>0;\ K>-J/2\}$, a doubly degenerate antiferromagnetic one in the region $\{J<0;\ K>J/2\}$, and a fourfold degenerate one with superantiferromagnetic (SAF) order in the remaining region $K<-|J|/2$. The SAF ground states consist of alternating rows of columns of up and down spins. In order to satisfy requirement (iii) of Sec. II, we shall *only* consider the flows in the subspace $K\geq 0$ in which we have only the FM and AFM ground states separated by the borderline of stability, $J=0$.

In three dimensions, we will study the simple cubic (sc) lattice which separates into two face-centered cubic (fcc) sublattices, and the body-centered cubic one (bcc) which separates into two simple cubic sublattices. Again, for reasons similar to those of the two-dimensional case, we will only examine the flows in the subspace $K\geq 0$; for both the sc and bcc models, the ground states are again FM for $J>0$ and AFM for $J<0$. We will present the calculation in some detail for the sq model only, and just describe the results for the sc and bcc cases, since the essential characteristics of the flows are quite similar for all three lattices.

A. Square lattice

For the sq model, we take as the small cluster the $N'=2$ spins joined by an elementary bond, and as the big

cluster the $N=4$ spins around an elementary plaquette of the lattice (Fig. 1). These are the two smallest clusters we are allowed to consider which satisfy the requirement of equivalence of the sublattice clusters. We take the points $A,C,\ldots$ forming the A sublattice and the points $B,D,\ldots$ forming the B sublattice. With the boundary magnetizations fixed to the values $b_1'(b_1)$ and $b_2'(b_2)$ for the A and B sublattices, we obtain the effective Hamiltonians

$$H'(s_A,s_B)=J'[s_As_B+3(s_Ab_2'+s_Bb_1')]+4K'(s_Ab_1'+s_Bb_2')+h'(s_A+s_B) \tag{3.2}$$

for the $N'=2$ cluster and

$$H(s_A,s_B,s_C,s_D)=J\{s_As_B+s_Bs_C+s_Cs_D+s_Ds_A+2[(s_A+s_C)b_2+(s_B+s_D)b_1]\}+$$
$$K\{s_As_C+s_Bs_D+3[(s_A+s_C)b_1+(s_B+s_D)b_2]\}+h(s_A+s_B+s_C+s_D) \tag{3.3}$$

for the $N=4$ cluster. Using Eqs. (3.2) and (3.3) above, we find the sublattice magnetizations per site as

$$m_A'=\frac{\sinh[(3J'+4K')(b_1'+b_2')+2h']-e^{-2J'}\sinh[(3J'-4K')(b_1'-b_2')]}{\cosh[(3J'+4K')(b_1'+b_2')+2h']+e^{-2J'}\cosh[(3J'-4K')(b_1'-b_2')]} \tag{3.4}$$

and

$$m_A=\{e^{4J+2K}\sinh[(4J+6K)(b_1+b_2)+4h]+2\sinh(4Jb_2+6Kb_1+2h)-$$
$$e^{-4J+2K}\sinh[(4J-6K)(b_1-b_2)]\}\times$$
$$\{e^{4J+2K}\cosh[(4J+6K)(b_1+b_2)+4h]+2\cosh(4Jb_2+6Kb_1+2h)+$$
$$2\cosh(4Jb_1+6Kb_2+2h)+e^{-4J+2K}\cosh[(4J-6K)(b_1-b_2)]+2e^{-2K}\}^{-1}\ . \tag{3.5}$$

Combining (2.3) and (2.4) with (3.4) and (3.5) above we obtain the $(J,K)\to(J',K')$ flows in the form

$$\frac{3J'+4K'-e^{-2J'}(3J'-4K')}{1+e^{-2J'}}$$
$$=\frac{4J+6K+12Ke^{-4J-2K}-e^{-8J}(4J-6K)}{1+4e^{-4J-2K}+e^{-8J}+2e^{-4J-4K}} \tag{3.6}$$

and

$$\frac{3J'+4K'+e^{-2J'}(3J'-4K')}{1+e^{-2J'}}$$
$$=\frac{4J+6K+8Je^{-4J-2K}+e^{-8J}(4J-6K)}{1+4e^{-4J-2K}+e^{-8J}+2e^{-4J-4K}}\ . \tag{3.7}$$

In the $K\geq 0$ subspace, the flows (3.6) and (3.7) have the fixed points (J_*,K_*) presented below.

(i) A stable low-temperature fixed point $L_1=(+\infty,+\infty)$ corresponding to the FM ground state.

(ii) A stable low-temperature fixed point $L_2=(-\infty,+\infty)$ corresponding to the AFM ground state.

(iii) A mixed low-temperature fixed point $L_3=(0,+\infty)$ which attracts along the $J=0$ direction only and repels in all other directions. This fixed point corresponds to the four degenerate FM and AFM configurations that are the ground states of the model, which, for $J=0$, reduces to two decoupled sq Ising models with nearest-neighbor coupling K.

(iv) A critical point $C_1=(0.1590,0.1499)$ which represents the ferromagnetic Ising criticality.

(v) A critical point $C_2=(-0.1590,0.1499)$ which represents the antiferromagnetic Ising criticality.

(vi) A multicritical point $C_3=(0,0.3465)$ which represents the criticality of the uncoupled sq Ising models described above.

(vii) The stable, high-temperature fixed point $P=(0,0)$

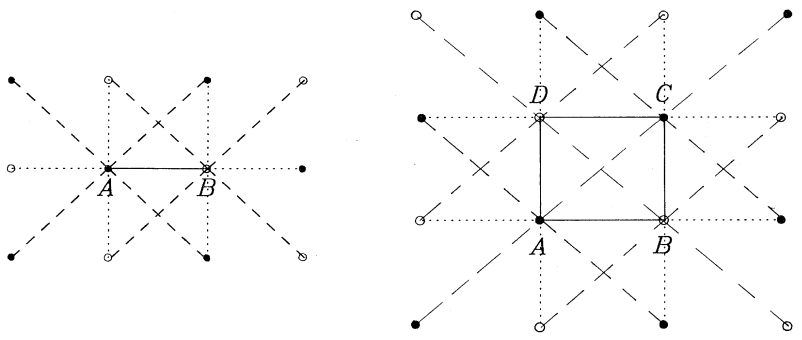

FIG. 1. The $N'=2$ and $N=4$ clusters used for the renormalization of the sq Ising Hamiltonian with crossing bonds. The fluctuating clusters are shown by solid lines. The filled dots form the A sublattice and the open ones the B sublattice.

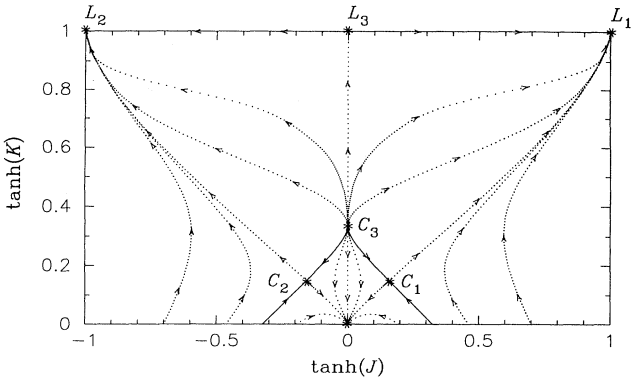

FIG. 2. RG flows of the sq Ising Hamiltonian with crossing bonds. The critical line is denoted by solid lines.

representing the paramagnetic phase.

The flows in the $K \geq 0$ subspace are shown in Fig. 2. We note that some of the flows emerge from two unstable fixed points located at $J=-2K, J \to +\infty$ and $J=2K, J \to -\infty$, located at the borderlines of stability of the ground states, which are not shown. As a first remark, we note that the flows are very similar to those obtained in the past by the use of other RG techniques [13,14], displaying reflection symmetry about the $J=0$ axis and a cusp of the critical surface at the point C_3. However, the RG flows are obtained here in a much simpler way, which is also readily generalizable to three-dimensional models in a very straightforward fashion. The flows are also similar to those obtained in earlier work by Plascak [11], but with the significant difference that here we avoid the ambiguities in the flows along the $J=0$ axis found in that work. In particular, we are able to obtain the multicritical fixed point C_3 *on the* $J=0$ *axis* which was missing in that approach, and on which, as we demonstrate below, certain important relations between the critical exponents are satisfied to a reasonable degree of accuracy. On the other hand, an obvious deficiency of our approach in its present formulation is that the theory is unable to locate the SAF critical fixed point at $J=0, K_* < 0$ since the way of separating the sublattices makes it inapplicable at present to the region in which the SAF fixed point lies.

For the calculation of the magnetic exponent y_h, a special treatment is required for the AFM fixed points. As can be seen from Eq. (2.6), when h is relevant, i.e., $y_h > 0$ (and $y_h > d/2$ of course) we have $\chi' < \chi$. On the other hand, when h is irrelevant and thus $y_h < 0$ we obtain the inequality $\chi' > \chi$. However, the last inequality itself only implies $y_h < d/2$, and not necessarily $y_h < 0$. Indeed, the sign of y_h is very sensitive to the choice of the rescaling factor s. In order to avoid complications related to the choice of this factor, and keep the discussion as simple as possible at present, we will characterize the magnetic field as irrelevant whenever we obtain $\chi' > \chi$, and this is indeed what we get at the AFM-criticality fixed point C_2.

For the low-temperature fixed points L_1 and L_3 we obtain the correct magnetic exponent $y_h = d$, a manifestation of a first-order phase transition [12]. For the point L_2 the magnetic field is irrelevant, whereas at the paramagnetic fixed point P we find correctly the result $y_h = d/2$. The locations of the $T>0$ critical points and the corresponding critical exponents are summarized in Table I.

TABLE I. The $T>0$ fixed points of the RG flows for the sq Ising model with crossing bonds presented in the text [Eqs. (3.6) and (3.7)] along with the corresponding critical exponents.

	(J_*, K_*)	y_1	y_2	$2y_h - d$
C_1	(0.1590,0.1499)	0.760	−1.023	0.974
C_2	(−0.1590,0.1499)	0.760	−1.023	−0.037
C_3	(0,0.3465)	1.073	0.600	0.830
P	(0,0)	−1.170	−0.830	0

The critical lines intersect the $K=0$ axis at the points $J_c = \pm 0.336$, which is the estimate from our theory for the FM and AFM critical couplings of the nearest-neighbor Ising model, to be compared with the exact result [15] $J_c = \pm 0.441$. This result is of the same quantitative accuracy as that obtained from the original MFRG with a $2 \to 1$ mapping, namely, $J_c = 0.346$; the latter is also the value of $K_* \equiv K_c$ at the fixed point C_3 which represents the FM criticality of the uncoupled sq Ising models with nearest-neighbor interactions *only*. The thermal exponent $y_1 = 0.760$ (at points C_1 and C_2) is in reasonable agreement with the exact result $y_t = 1$, and the magnetic exponent $y_h = 1.487$ differs from the exact one $y_h = \frac{15}{8}$ by about 20%.

At the multicritical fixed point C_3 we have an exponent $y_1 = 1.073$ with the corresponding eigenvector along the (1,0) direction and an exponent $y_2 = 0.600$ with the corresponding eigenvector along the (0,1) direction. This allows us to identify the latter with the thermal exponent y_t of the uncoupled Ising lattices, and we call $y_1 = y_s$ to comply with the terminology introduced in Ref. [14]. As a first remark, we note that y_t differs from the thermal exponent y_1 for the points C_1 and C_2, but this is not surprising in view of the fact that our method is a $4 \to 2$ mapping in general, but for $J=0$ it reduces effectively to a $2 \to 1$ mapping; different degrees of approximation in the mappings yield different estimates for the critical exponents, as expected. On the other hand, the magnetic exponent $y_h = 1.415$ at C_3 is not too different from $y_h = 1.487$ at C_1 and C_2. According to van Leeuwen [14] the exponents y_s and y_t must satisfy the relations

$$y_s = 2y_h - d \tag{3.8}$$

and

$$y_s / y_t = \gamma_{\text{Ising}} \, . \tag{3.9}$$

Using the results in Table I, we find that the right-hand side (RHS) of (3.8) is equal to 0.830, whereas the LHS is 1.073, which shows once more that the critical exponents are not evaluated very accurately in the MFRG, at least with small clusters and with the naive definition of s; however, the ratio y_s / y_t is equal to 1.789, and the exact

TABLE II. The $T>0$ fixed points of the RG flows for the sc Ising model with crossing bonds and the corresponding exponents.

	(J_*,K_*)	y_1	y_2	$2y_h-d$
C_1	(0.0629,0.0580)	0.506	−0.424	0.552
C_2	(−0.0629,0.0580)	0.506	−0.424	−0.056
C_3	(0,0.0912)	0.443	0.344	0.376
P	(0,0)	−0.966	−0.377	0

result for the RHS of (3.9) is $\gamma_{\text{Ising}}=1.75$, which shows that *ratios* of the critical exponents come out rather accurately in this approach, since they are independent of the precise definition of the rescaling factor.

We now extend the approach to three dimensions, studying the flows for the simple cubic and body-centered cubic models, always in the subspace $K\geq 0$.

B. Simple cubic lattice

For the sc lattice the two clusters are again the elementary bond ($N'=2$) and the elementary plaquette ($N=4$), once more the smallest possible clusters which satisfy the requirements of the approach. The low- and high-temperature fixed points L_1, L_2, L_3, and P are identical to those in the sq case, also with the correct magnetic exponents. Once more, we find the two critical points C_1 and C_2 and the multicritical point C_3 whose coordinates and critical exponents are summarized in Table II. The overall flow pattern is identical to that in the sq case.

The critical lines now intersect the $K=0$ axis at the points $J_c=\pm 0.192$, to be compared with the "exact" result [15] $J_c=\pm 0.222$. At the critical points C_1 and C_2 we find the thermal exponent $y_1=0.506$ which differs quite a bit from the "exact" result [16] $y_t=1.587$; the magnetic exponent $y_h=1.776$ is somewhat closer to the value [16] $y_h=2.485$. The value K_* of the point C_3 gives an estimate of the critical coupling of the fcc nearest-neighbor Ising model, since for $J=0$ the model decouples into the two independent fcc sublattices of the sc lattice. We obtain $K_c\equiv K_*=0.091$ to be compared with the estimate [15] $K_c=0.102$. We note in passing that the MFRG inherits from the underlying mean-field ideas the characteristic that the values of the critical couplings improve, for the same degree of approximation, as the coordination number of the lattice increases. The value of the thermal exponent, however, does not: at the point C_3, $y_t\equiv y_2=0.344$, which is worse than the values at C_1 and C_2; ideally, all these estimates should converge to the exact three-dimensional (3D) Ising values as one considers larger and larger clusters. The magnetic exponent at C_3, $y_h=1.688$, is again not too different from its value at C_1. Regarding the relation (3.8) we obtain 0.443 for the LHS and 0.377 for the RHS, whereas the ratio $y_s/y_t=1.288$ is not too far away from the "exact" value $\gamma_{\text{Ising}}=1.238$ (Ref. [17]) required from Eq. (3.9). Again, the ratio of the critical exponents is very accurate, although the individual exponents are not.

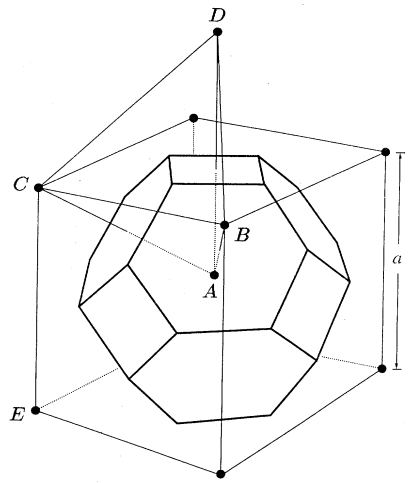

FIG. 3. A local arrangement of the bcc lattice and the bcc Wigner-Seitz unit cell.

C. Body-centered cubic lattice

Here, the small cluster is chosen to be the nearest-neighbor bond ($N'=2$). For the larger cluster, there are two $N=4$ choices that satisfy the requirements: the $ABCD$ tetrahedron and the $ADCE$ parallelogram shown in Fig. 3. Both mappings yield identical low- and high-temperature fixed points, with the correct magnetic exponents. Moreover, they yield the same multicritical point $C_3=(0,0.203)$ but they differ slightly in the non-magnetic critical exponents at C_3 as well as at the locations and exponents of the critical points C_1 and C_2. The flow patterns are again very similar to those presented above for the other lattices. Although the critical fixed points are different, the *critical lines* from the two mappings are almost identical. This demonstrates that the method is robust (insensitive) to the choice of the large cluster.

The results are summarized in Tables III(a) and III(b). The value $K_*=0.203$ at the fixed point C_3 is an estimate for the critical coupling of the sc Ising model with nearest-neighbor coupling, again not too far from the exact value 0.222 and the previous sc estimate 0.192. The critical lines now intersect the $K=0$ axis at the points $J_c=\pm 0.140$ for the tetrahedron $\rightarrow$ bond mapping and $J_c=\pm 0.139$ for the parallelogram $\rightarrow$ bond mapping which are the estimates for the bcc Ising critical coupling, to be compared with the best estimate [15] $J_c=\pm 0.157$. A comparison of the critical exponents with the exact ones shows that the tetrahedron $\rightarrow$ bond mapping yields better results not only in terms of their numerical values, but also in the sense that it predicts almost identical values for the thermal and magnetic exponents for the points C_1 and C_3, as required by universality. The relations (3.8) and (3.9) are satisfied within an error of at most 10%.

The above discussion demonstrates that the RG method we propose here yields very satisfactory results

TABLE III. (a) The $T>0$ fixed points of the RG flows for the bcc Ising model with crossing bonds and the corresponding exponents obtained from the tetrahedron→bond mapping; (b) same as part (a) but using the parallelogram→bond mapping.

	(J_*,K_*)	y_1	y_2	$2y_h-d$
		(a)		
C_1	(0.0781,0.0791)	0.653	−0.848	0.724
C_2	(−0.0781,0.0791)	0.653	−0.848	−0.061
C_3	(0,0.2027)	0.901	0.650	0.788
P	(0,0)	−0.667	−0.789	0
		(b)		
C_1	(0.0994,0.0494)	0.426	−0.800	0.466
C_2	(−0.0994,0.0494)	0.426	−0.800	−0.026
C_3	(0,0.2027)	0.846	0.650	0.788
P	(0,0)	−0.320	−0.789	0

for some standard "test" models, and thus it is a plausible technique for the renormalization of more complicated Hamiltonians.

IV. MORPHOLOGICAL MODEL

We consider in this section a phenomenological morphological Hamiltonian on a bcc lattice, introduced recently in order to model the phase behavior of microemulsions [6]. Here, we outline the basic ideas in the derivation of the model, and refer the reader to Ref. [6] for details. Let us consider a three-dimensional Bravais lattice with periodic boundary conditions, having N sites and volume V, whose Wigner-Seitz (WS) unit cells contain either bulk water or oil. In addition, the system contains amphiphilic molecules which are supposed to form an incompressible membrane in the interface between oil and water, defining in this way a Gibbs dividing surface between the two bulk phases. After choosing an orientation for this interface, a collection of water cells fixes uniquely an interfacial pattern, and vice versa. We denote a cell to be "occupied" if it contains water, and "empty" if it contains oil. The morphological features of each pattern can be described by the Minkowski functionals; in three dimensions, these are the geometric invariants: covered volume, surface area, integral mean curvature of the interface, and the combinatorial Euler characteristic X of the pattern. We have $X=$(number of disconnected components)−(number of handles) +(number of cavities) in three dimensions. In the present model the interfaces have no holes. The family of the Minkowski functionals is characterized by a theorem which asserts that any real-valued, additive, motion-invariant, and continuous functional defined on the collection of the 2^N configurations is a linear combination of the Minkowski functionals. [18,19]. In order to deal with the statistical morphology of the interfacial membrane, we therefore take the Hamiltonian to be of the generic form:

$$\mathcal{H}=\sum_{\alpha=0}^{3} h_\alpha V_\alpha \ , \tag{4.1}$$

where h_α are energy parameters and V_α are, within proportionality factors, the dimensionless Minkowski functionals as follows: denoting by $\mathcal{V}$, $\mathcal{A}$, $\mathcal{M}$, and X the covered volume, exposed area, integral mean curvature, and Euler characteristic of the pattern formed by the full cells, we have $V_0=\mathcal{V}/(8\sqrt{2}l^3)$, $V_1=\mathcal{A}/[3(4\sqrt{2}+2)l^2]$, $V_2=\mathcal{M}/(6\pi l)$, and $V_3=X$. The various factors arise from the definition of the Minkowski functionals via Steiner's formula, and their values for the bcc WS polyhedron (see the Appendix and Table I of Ref. [6]). The length scale l is the edge length of the WS unit cell of the bcc lattice, $l=a\sqrt{2}/4$, where a is the bcc lattice constant (see Fig. 3).

Using the property of additivity, one can derive concise expressions for the Minkowski functionals in terms of the occupation numbers $u_i=0,1$ ($u_i=0$ if the cell is occupied, $u_i=1$ if it is empty) and in Ref. [6] the Hamiltonian was written down explicitly in that representation. Here, it will be more useful to write the Hamiltonian in terms of "Ising spin" variables $s_i=\pm 1$, with $s_i=1$ denoting a full site and $s_i=-1$ an empty one (i.e., $s_i=1-2u_i$). Setting $\mathbf{s}=(s_1,s_2,\ldots,s_N)$, the final expression reads as

$$\begin{aligned}\mathcal{H}(\mathbf{s})=\sum_{\alpha=0}^{3} h_\alpha V_\alpha(\mathbf{s})=h_0\left[\frac{N}{2}+\tfrac{1}{2}\sum_i s_i\right]+\\ \frac{h_1}{4}\left[N-\frac{\sqrt{3}}{4\sqrt{3}+2}\sum{}' s_i s_j-\frac{2}{3(4\sqrt{3}+2)}\sum{}'' s_i s_j\right]+\\ \frac{h_2}{4}\left[-\sum_i s_i+\tfrac{1}{12}\sum{}''' s_i s_j s_k\right]+\frac{h_3}{8}\left[-N+\sum{}' s_i s_j-\tfrac{1}{2}\sum{}'''' s_i s_j s_k s_l\right] .\end{aligned} \tag{4.2}$$

The primed and double-primed sums are carried over nearest- and next-nearest-neighbor bonds, respectively. The triple-primed sum runs over isosceles triangles, two of the sides of the triangles being first-neighbor bonds and the third being a second-neighbor bond. Such are the *ABC*, *BCD*, *ABD*, and *ACD* triangles in Fig. 3, for instance. Finally, the four-primed sum runs over tetrahedra whose faces are isosceles triangles as above, e.g., the *ABCD* tetrahedron of Fig. 3. Under the interchange $s_i\to -s_i$, the integral mean curvature is odd, whereas the exposed area and Euler characteristic are even.

We are going to deal exclusively with the case $h_2=0$

(no spontaneous internal curvature.) For $h_0=h_2=0$, the ground states (GS's) of the model are the following: a doubly degenerate ferromagnetic GS (oil or water, OW) in the region

$$\left\{h_3<\frac{\sqrt{3}}{2\sqrt{3}+1}h_1;h_3>-h_1\right\}; \tag{4.3}$$

a doubly degenerate antiferromagnetic GS [("plumber's nightmare," (PN)] in the region

$$\left\{h_3>\frac{\sqrt{3}}{2\sqrt{3}+1}h_1;h_3>\frac{2\sqrt{3}-1}{5(2\sqrt{3}+1)}h_1\right\}; \tag{4.4}$$

and a fourfold degenerate "droplet" phase in the region

$$\left\{h_3<-h_1;h_3<\frac{2\sqrt{3}-1}{5(2\sqrt{3}+1)}h_1\right\}. \tag{4.5}$$

The "plumber's nightmare" is an ordered, cubic phase characterized by a structure of interwoven, coherent oil and water tubes, separated by a layer of amphiphiles. The droplet phase is realized when one of the two sc sublattices has ferromagnetic and the other antiferromagnetic order. The subspace $h_3>0$ is covered completely by the OW and PN ground states, separated by the borderline of stability $h_1=(2\sqrt{3}+1)h_3/\sqrt{3}$; thus, according to the general requirements laid out in Sec. II, we are going to consider the flows in the subspace $h_3\geq 0$ only [20].

Dropping the uninteresting spin-independent constants from the Hamiltonian, and defining

$$h=-\frac{\beta h_0}{2},\quad J=\frac{\beta h_1}{24(4\sqrt{3}+2)},\quad K=\frac{\beta h_3}{16}, \tag{4.6}$$

we arrive at the expression

$$H\equiv-\beta\mathcal{H}=h\sum_i s_i+(6\sqrt{3}J-2K)\sum{}' s_is_j +4J\sum{}'' s_is_j+K\sum{}'''' s_is_js_ks_l\ . \tag{4.7}$$

For the choice $h_3=0$ the model reduces to a conventional bcc Ising model with an additional second-neighbor coupling, namely,

$$H=h\sum_i s_i+L\sum{}' s_is_j+\alpha L\sum{}'' s_is_j\ , \tag{4.8}$$

where $L=\beta\sqrt{3}h_1/(16\sqrt{3}+8)$ and $\alpha=2/(3\sqrt{3})$ is the ratio of second- to first-neighbor coupling.

We are now interested in the renormalization of Hamiltonian (4.2). When $h_0=h_2=0$ a real-space RG will generate flows with at least three parameters corresponding to the three even interactions in (4.7), whereas the initial morphological Hamiltonian (4.1) contains only two, h_1 and h_3 [or J and K in (4.6) and (4.7)] in the even subspace. However, after coarse graining the effective Hamiltonian must still be additive, motion invariant, and continuous like the initial one. Thus it must be again a linear combination of the Minkowski functionals, i.e., of the form (4.1). Our extension of the MFRG allows us to impose this requirement quite naturally, by assuming that the renormalized Hamiltonian for the N' cluster always has the form (4.7).

Clearly, the model satisfies all prerequisites of Sec. II, and we can proceed with the EMFRG approach. We choose for the small cluster the AB bond ($N'=2$) and for the large one the $ABCD$ tetrahedron ($N=4$) shown in Fig. 3. The points $A,D,\ldots$ form the A sublattice and the points $B,C,\ldots$ form the B sublattice. Some details of the derivation of the flows are given in the Appendix. The flow equations read as

$$\begin{aligned}&\frac{(42\sqrt{3}J'-14K')\sinh(6\sqrt{3}J'-2K')+24J'\cosh(6\sqrt{3}J'-2K')}{\cosh(6\sqrt{3}J'-2K')}\\&=\left\{e^{(24\sqrt{3}+8)J-7K}[(72\sqrt{3}+40)J-22K]+2e^{-K}(40J-2K)-\right.\\&\left.e^{(-24\sqrt{3}+8)J+9K}[(72\sqrt{3}-40)J-26K]\right\}\times\\&\left\{e^{(24\sqrt{3}+8)J-7K}+4e^{-K}+2e^{-8J+K}+e^{(-24\sqrt{3}+8)J+9K}\right\}^{-1}\end{aligned} \tag{4.9}$$

and

$$\begin{aligned}&\frac{(42\sqrt{3}J'-14K')\cosh(6\sqrt{3}J'-2K')+24J'\sinh(6\sqrt{3}J'-2K')}{\cosh(6\sqrt{3}J'-2K')}\\&=\left\{e^{(24\sqrt{3}+8)J-7K}[(72\sqrt{3}+40)J-22K]+2e^{-K}(72\sqrt{3}J-24K)+\right.\\&\left.e^{(-24\sqrt{3}+8)J+9K}[(72\sqrt{3}-40)J-26K]\right\}\times\\&\left\{e^{(24\sqrt{3}+8)J-7K}+4e^{-K}+2e^{-8J+K}+e^{(-24\sqrt{3}+8)J+9K}\right\}^{-1}.\end{aligned} \tag{4.10}$$

The above flows have in the subspace $K \geq 0$ the fixed points (J_*, K_*) listed below.

(i) A stable low-temperature fixed point $L_1 = (+\infty, +\infty)$ representing the ferromagnetic (OW) ground state.

(ii) A stable low-temperature fixed point $L_2 = (-\infty, +\infty)$ representing the antiferromagnetic (PN) ground state.

(iii) A mixed low-temperature fixed point $L_3 = (J_*, 3\sqrt{3}J_*)$ with $J_* \to +\infty$. This point attracts in the direction $K = 3\sqrt{3}J$ [i.e., $h_3 = \sqrt{3}h_1/(2\sqrt{3}+1)$] and repels in the other directions. It corresponds to the fourfold degenerate ground states of the model when the couplings h_1 and h_3 have the ratio given above, and in which case the first-neighbor coupling vanishes; then, the OW and PN phases are all degenerate at $T=0$.

(iv) A critical point $C_1 = (1.656\times10^{-2}, 5.306\times10^{-2})$ which represents the Ising ferromagnetic criticality.

(v) A critical point $C_2 = (1.407\times10^{-2}, 9.858\times10^{-2})$ which represents the Ising antiferromagnetic criticality.

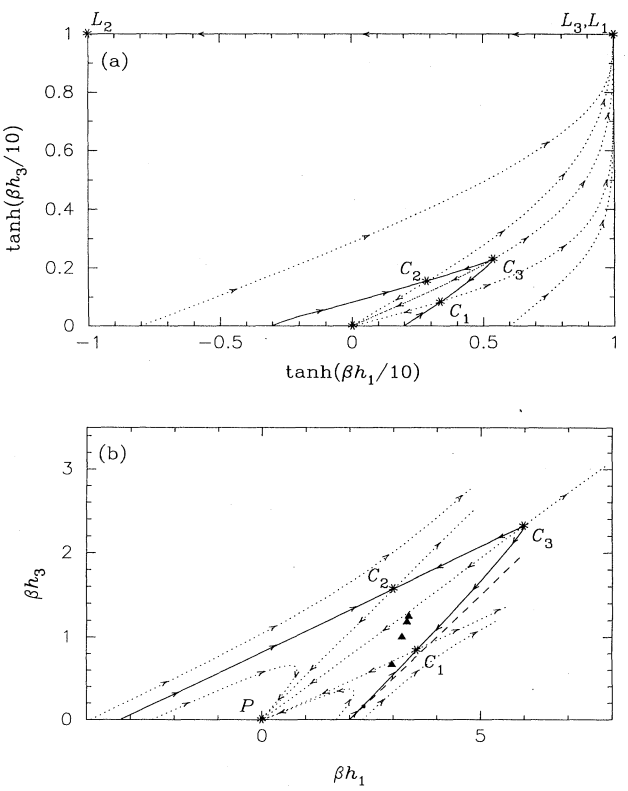

FIG. 4. RG flows of the bcc morphological Hamiltonian: (a) throughout the subspace $h_3 \geq 0$ and (b) in more detail, in the neighborhood of the critical points. The lines along which the critical points C_1 and C_2 attract are denoted solid. The dashed line is the locus of vanishing inverse susceptibility from the simple mean-field approximation. The mean-field tricritical point is indicated by the dot. The filled triangles denote values of the energy parameters for which the mean-field approximation yields three-phase coexistence between oil-rich, water-rich, and a middle, random, bicontinuous microemulsion.

(vi) A multicritical point $C_3 = (2.785\times10^{-2}, 1.447\times10^{-1})$.

(vii) The high-temperature, stable fixed point $P=(0,0)$ representing the paramagnet.

The flows are shown in Fig. 4(a); due to the particular representation chosen to show the flows, the fixed points L_1 and L_3 coincide in this figure. We obtain the correct magnetic exponent $y_h = d$ at L_1 and L_3 and $y_h = d/2$ at P. The subspace $h_3 = \sqrt{3}h_1/(2\sqrt{3}+1)$ is an eigenspace of the flows, with the fixed point C_3 lying in this subspace. Flows that start in this space remain in it, running towards the point L_3 if they start above C_3 or towards the point P if they start below C_3. Thus, in the special case of a model with vanishing first-neighbor coupling, the flows maintain that property. The parameter space is thus separated into three basins of attraction [see Fig. 4(a)]. Flows starting in the region enclosed in the "triangle" formed by the two critical lines and the axis $h_3=0$ run towards the P point. Flows starting outside the triangle and on the right of the line P-C_3-L_3 run to the OW fixed point L_1, always remaining in the region $h_3 < \sqrt{3}h_1/(2\sqrt{3}+1)$; and flows that start outside the triangle but on the left of the line P-C_3-L_3 run initially close to L_3, but eventually they turn around to end up in the PN fixed point L_2, staying always in the subspace $h_3 > \sqrt{3}h_1/(2\sqrt{3}+1)$.

The locations of the $T>0$ fixed points and the associated critical exponents are summarized in Table IV. We note that the method predicts identical values for the thermal exponent y_1 for both ferromagnetic and antiferromagnetic Ising critical points, as it should. The value $y_1 = 0.691$ is comparable to the value $y_1 = 0.653$ obtained for the bcc Ising model with crossing bonds using the same kind of mapping (tetrahedron$\to$bond) discussed in Sec. III [see Table III(a)]. As further evidence for the consistency of the method, we note that the critical line of the C_1 fixed point intersects the $h_3=0$ axis at the point $\beta h_1^c = 2.019$ [see Fig. 4(b)]. Accordingly, the critical coupling of the Hamiltonian (4.8) (to which the model reduces in the case $h_3=0$) is predicted to be $L_c = 0.098$. On the other hand, the line corresponding to $\alpha = 2/(3\sqrt{3})$ intersects the critical line of the ferromagnetic fixed point C_1 of the bcc Hamiltonian studied in Sec. III at a point whose abscissa is equal to 0.105. The two estimates differ by less than 7%.

In order to obtain more detailed information about the phase behavior of the model, we have to invoke the results from other techniques as well, for example, from the simple mean-field approximation. The reason is that the

TABLE IV. The $T>0$ fixed points of the RG flows for the morphological Hamiltonian and the corresponding exponents.

	(J_*, K_*)	y_1	y_2	$2y_h - d$
C_1	$(1.656\times10^{-2}, 5.306\times10^{-2})$	0.691	−0.740	0.646
C_2	$(1.407\times10^{-2}, 9.858\times10^{-2})$	0.691	−0.610	−0.029
C_3	$(2.785\times10^{-2}, 1.447\times10^{-1})$	0.728	0.564	0.516
P	(0,0)	−0.667	−0.789	0

proposed RG scheme has certain limitations due to the feature of always expanding the cluster magnetization around vanishingly small expectation values $\langle s_i \rangle$ of the surrounding spins. Consequently, not all of the points lying on the "critical lines" correspond to true criticalities. Let us consider, for instance, the mean-field expression for the free energy per site which reads as [6]

$$\beta f(m)=\frac{\beta h_1}{4}(1-m^2)+\frac{\beta h_3}{8}(-1+4m^2-3m^4)+\frac{1+m}{2}\ln\left[\frac{1+m}{2}\right]+\frac{1-m}{2}\ln\left[\frac{1-m}{2}\right], \tag{4.11}$$

where $m=\langle s_i \rangle$. Expanding the free energy about $m=0$ up to $O(m^4)$ and dropping the uninteresting constants, we obtain

$$\beta f(m)=\left[-\frac{\beta h_1}{4}+\frac{\beta h_3}{2}+\frac{1}{2}\right]m^2+\left[-\frac{3\beta h_3}{8}+\frac{1}{12}\right]m^4 . \tag{4.12}$$

The requirement of vanishing coefficient of the quadratic term identifies the line of diverging susceptibility, $\chi^{-1}=0$, and reads as

$$\beta h_3=\frac{\beta h_1-2}{2} . \tag{4.13}$$

However, not all the points defined by (4.13) correspond to tue criticalities, which happen only when the coefficient of the m^4 term is positive. This requirement yields a tricritical point $(\beta h_1^{\rm tr}, \beta h_3^{\rm tr})=(\frac{22}{9},\frac{2}{9})$. In Fig. 4(b) we plot the line (4.13) along with the flows and indicate the tricritical point by a dot. We note that below the dot the attractive line of the fixed point C_1 almost coincides with (4.13). The true tricritical point of the model must occur at a temperature lower than the mean-field prediction, of course, but taking for now the estimate for tricriticality from the mean-field approximation for granted, we can give to the attractive line of the point C_1 the following interpretation: the segment of the line below the dot corresponds to true criticality. However, the part of the solid line above the dot does not represent a line of critical points, but rather a line of diverging susceptibility at $m=0$ which, however, does not correspond to true criticalities because these are preempted by the phase coexistence between oil-rich and water-rich phases [21]. The inability of the present RG scheme to distinguish between a critical line and a line of preempted criticalities lies in the expansions of the magnetizations about vanishingly small values of the boundary spins, i.e., in the assumption that the system is translationally invariant and has a vanishingly small bulk magnetization. Similar considerations also apply to the C_2 "critical line."

Another feature of the model found in the mean-field approximation and confirmed by extensive Monte Carlo simulations [6] is the possibility of *three-phase coexistence* between oil-rich, water-rich, and a middle disordered phase, characterized as a microemulsion in view of its morphological (negative Euler characteristic) and structural (a peak of the structure factor at nonzero wave vector) properties. The three-phase coexistence is caused by the competition between a positive surface tension $\beta h_1 \sim 1$ of the incompressible surfactant film, which tends to minimize the exposed area, and a positive topological potential $\beta h_3 \sim 1$ which encourages structures with a large surface area in order to accommodate many handles, and thus it assists the entropic tendency to disperse the amphiphiles. The microemulsion has a finite correlation length ξ of the order of a few lattice constants, i.e., it displays short-range order (unlike the completely random mixture, or "paramagnet" in the magnetic language). Clearly, since ξ is neither vanishing nor diverging, the microemulsion is not represented by a fixed point in the flow diagram. We must, therefore, resort once more to external information in order to identify the region in the flow diagram which represents stable microemulsion phases. According to earlier work [6], the middle phase occurs in a range of temperatures $0.80 \lesssim k_B T/h_3 \leq \frac{9}{2}$, the upper limit being the tricritical temperature, above which three-phase coexistence ceases to exist. On the other hand, below the lower limit the middle phase again disappears because it is replaced by a slightly disordered "plumber's nightmare" phase. We take the combinations of the energy coefficients that give a three-phase coexistence as "pointers" that indicate the region on the flow diagram where the microemulsion is stable. In Fig. 4(b) we mark a few of those points, which are once more obtained from the mean-field approximation; the latter has been found to be relatively accurate in its predictions for the triple points, when compared to the simulation results [6]. Referring to this figure, we can now assert that the neighborhood of the filled triangles below the PC_3 line, to the left of the solid line, and above the tricritical point roughly defines the domain of thermodynamic stability of the microemulsion. Clearly, upon coarse graining all points in the microemulsion regime flow towards the paramagnet. In order to delimit the region of stability of the microemulsion more accurately, one could, for example, study the small wave number behavior of the Fourier transform of the correlation function within the RG scheme. However, such a calculation lies beyond the scope of this work.

V. SUMMARY AND CONCLUSIONS

We have presented a generalization of the mean-field renormalization group method which provides a way of renormalizing Hamiltonians with two coupling constants in the even interaction part. The method builds on ideas which are similar to those of the original MFRG, but it goes beyond the limitation of a single flow equation by employing scaling assumptions about suitably chosen sublattice magnetizations. We applied the method to several model Hamiltonians, obtaining satisfactory results for the flow diagrams. An obvious challenge for the future is the development of these ideas even further, so that we will be able to deal with Hamiltonians involving

more than two parameters. A possible way to achieve this goal will be through a separation of the lattice into more than just two suitably chosen sublattices; however, since the EMFRG always yields as many flow equations as sublattices, it may be necessary in some cases to augment the original Hamiltonian by a suitably chosen number of interactions and coupling constants until the number of couplings matches the number of sublattices. Then, the flows would be obtained in this enlarged parameter space, and one could look at the flows in the original, restricted domain by taking the appropriate "cuts" in Hamiltonian space.

The morphological model of Sec. IV includes all additive geometrical invariants whose thermal averages are extensive. The manifest additivity of the Hamiltonian is a sufficient, but not necessary, condition for the thermodynamic requirement of extensivity of the internal energy. Therefore, one should not exclude *a priori* terms in the Hamiltonian which are not additive; in particular, a nonadditive "curvature-square" term, which is employed in most current models of microemulsions, is missing from the Hamiltonian. In the original paper [6], it was argued that the model deals with length scales exceeding the persistence length [22] ξ_κ, where the above contribution (also called the "bending energy") can be omitted because the scale-dependent bending rigidity has been renormalized away. A nonperturbative renormalization of a Hamiltonian including the surface area and bending energy terms only was presented recently [23]; our model is complementary to that of Ref. [23] in that it includes the Euler characteristic term, but not the bending rigidity. It would be desirable, therefore, to start with a Hamiltonian that includes the Minkowski functionals *and* the bending energy and proceed with its renormalization, in order to see the crossover from the rigidity-dominated regime (for lengths scales below ξ_κ) to the regime above ξ_κ where the thermal fluctuations dominate over the rigidity and the membrane is crumpled. We plan to return to this problem in the future.

ACKNOWLEDGMENTS

We wish to thank Professor H. Wagner for suggesting this problem to one of us (C.N.L.) and for helpful discussions. This work was started while C.N.L. was at the Sektion Physik der Ludwig-Maximilians-Universität München. C.N.L. wishes to thank the Alexander von Humboldt–Stiftung for financial support throughout his stay in Munich, and also acknowledges the support by the Human Capital and Mobility Programme of the Commission of the European Communities, Contract No. ERBCHBICT940940, during his stay in Trieste.

APPENDIX

Here we outline the steps for the derivation of the flow equations for the morphological Hamiltonian of Sec. IV, Eq. (4.7). Consider first the small cluster AB, $N'=2$. Fixing all the surrounding $A(B)$ sublattice spins to the value b_1' (b_2'), and using (4.7) and Fig. 3, we arrive at the effective Hamiltonian of the $N'=2$ cluster of the form

$$H'(s_A,s_B)=h'S_0'+(6\sqrt{3}J'-2K')S_1'+4J'S_2'+K'S_4' , \tag{A1}$$

where

$$S_0'=s_A+s_B , \tag{A2}$$

$$S_1'=s_As_B+7(s_Ab_2'+s_Bb_1') , \tag{A3}$$

$$S_2'=6(s_Ab_1'+s_Bb_2') , \tag{A4}$$

and

$$S_4'=6b_1'b_2'[s_As_B+3(s_Ab_2'+s_Bb_1')] . \tag{A5}$$

Similarly, the effective Hamiltonian for the $ABCD$ cluster ($N=4$) has the form

$$H(s_A,s_B,s_C,s_D)=hS_0+(6\sqrt{3}J-2K)S_1+4JS_2+KS_4 , \tag{A6}$$

where

$$S_0=s_A+s_B+s_C+s_D , \tag{A7}$$

$$S_1=s_As_B+s_Bs_D+s_Ds_C+s_Cs_A +6[(s_A+s_D)b_2+(s_B+s_C)b_1] , \tag{A8}$$

$$S_2=s_As_D+s_Bs_C+5[(s_A+s_D)b_1+(s_B+s_C)b_2] , \tag{A9}$$

and

$$S_4=s_As_Bs_Cs_D+s_Bs_C(s_A+s_D)b_1+s_As_D(s_B+s_C)b_2+ 3(s_As_B+s_Bs_D+s_Ds_C+s_Cs_A)b_1b_2+s_As_Db_2^2+s_Bs_Cb_1^2+ 13b_1b_2[(s_A+s_D)b_2+(s_B+s_C)b_1] . \tag{A10}$$

Using the above expressions, and ignoring terms of order $(b')^2$ and b^2 which do not contribute anything to the flow equations, we find the sublattice magnetizations per site as

$$\begin{aligned} m_A'=&(e^{6\sqrt{3}J'-2K'}\sinh\{[(42\sqrt{3}+24)J'-14K'](b_1'+b_2')\}+ \\ &e^{-6\sqrt{3}J'+2K'}\sinh\{[(42\sqrt{3}-24)J'-14K'](b_2'-b_1')\}) \\ &\times(e^{6\sqrt{3}J'-2K'}\cosh\{[(42\sqrt{3}+24)J'-14K'](b_1'+b_2')\}+ \\ &e^{-6\sqrt{3}J'+2K'}\sinh\{[(42\sqrt{3}-24)J'-14K'](b_2'-b_1')\})^{-1} \end{aligned} \tag{A11}$$

for the small cluster, and

$$m_A = (e^{(24\sqrt{3}+8)J-7K}\sinh\{[(72\sqrt{3}+40)J-22K](b_1+b_2)\}+$$
$$2e^{-K}\sinh\{(72\sqrt{3}J-24K)b_2+(40J-2K)b_1\}+$$
$$e^{(-24\sqrt{3}+8)J+9K}\sinh\{[(72\sqrt{3}-40)J-26K](b_2-b_1)\})\times$$
$$(e^{(24\sqrt{3}+8)J-7K}\cosh\{[(72\sqrt{3}+40)J-22K](b_1+b_2)\}+$$
$$2e^{-K}\cosh\{(72\sqrt{3}J-24K)b_2+(40J-2K)b_1\}+$$
$$2e^{-K}\cosh\{(72\sqrt{3}J-24K)b_1+(40J-2K)b_2\}+$$
$$2e^{-8J+K}+e^{(-24\sqrt{3}+8)J+9K}\cosh\{[(72\sqrt{3}-40)J-26K](b_2-b_1)\})^{-1} \tag{A12}$$

for the large cluster (where we have set $h'=h=0$). Differentiation of Eqs. (A11) and (A12) with respect to b_1' and b_2' and b_1 and b_2 leads to the flow equations (4.9) and (4.10) of the main text. The zero-field susceptibilities needed for the calculation of the magnetic exponent read as

$$\chi_*' = \frac{e^{6\sqrt{3}J_*-2K_*}}{\cosh(6\sqrt{3}J_*-2K_*)} \tag{A13}$$

and

$$\chi_* = \frac{4[e^{(24\sqrt{3}+8)J_*-7K_*}+e^{-K_*}]}{e^{(24\sqrt{3}+8)J_*-7K_*}+4e^{-K_*}+2e^{-8J_*+K_*}+e^{(-24\sqrt{3}+8)J_*+9K_*}} . \tag{A14}$$

[1] J. O. Indekeu, A. Maritan, and A. L. Stella, J. Phys. A **15**, L291 (1982).

[2] For a recent review, see A. Croes and J. O. Indekeu, Mod. Phys. Lett. B **7**, 699 (1993).

[3] J. O. Indekeu, A. L. Stella, and L. Zhang, J. Phys. A **17**, L341 (1984).

[4] P. A. Slotte, J. Phys. A **20**, L177 (1987).

[5] J. O. Indekeu, A. Maritan, and A. L. Stella, Phys. Rev. B **35**, 305 (1987).

[6] C. N. Likos, K. R. Mecke, and H. Wagner, J. Chem. Phys. **102**, 9350 (1995).

[7] M. P. Nightingale, Physica A **83**, 561 (1976).

[8] M. N. Barber, Physica A **130**, 171 (1985).

[9] P. M. C. de Oliveira and F. C. Sá Baretto, J. Stat. Phys. **57**, 53 (1989).

[10] J. Ashkin and E. Teller, Phys. Rev. **64**, 178 (1943).

[11] J. A. Plascak, Physica A **183**, 563 (1992).

[12] Th. Niemeijer and J. M. J. van Leeuwen, in *Phase Transitions and Critical Phenomena,* edited by C. Domb and M. S. Green (Academic, London, 1976), Vol. 6.

[13] M. Nauenberg and B. Nienhuis, Phys. Rev. Lett. **33**, 944 (1974).

[14] J. M. J. van Leeuwen, Phys. Rev. Lett. **34**, 1056 (1975).

[15] C. Domb, in *Phase Transitions and Critical Phenomena,* edited by C. Domb and M. S. Green (Academic, London, 1974), Vol. 3.

[16] J. C. Le Guillou and J. Zinn-Zustin, Phys. Rev. B **21**, 3976 (1980).

[17] G. S. Pawley, R. H. Swendsen, D. J. Wallace, and K. G. Wilson, Phys. Rev. B **29**, 4030 (1984).

[18] H. Hadwiger, *Vorlesungen über Inhalt, Oberfläche und Isoperimetrie* (Springer, Berlin, 1957).

[19] W. Weil, in *Convexity and its Applications,* edited by P. M. Gruber and J. M. Wills (Birkhäuser, Basel, 1983).

[20] In Ref. [6] above, the model was also exclusively studied for the case $h_3>0$. The reason for that choice was that $h_3>0$ puts large statistical weights on configurations with negative Euler characteristic and thus encourages the stability of phases with a random, bicontinuous nature, such as microemulsions.

[21] It has to be expected that *only* part of the "critical line" can be preempted since, for small values of h_3, the model is a slightly perturbed Ising model and the order of the phase transition remains unchanged.

[22] P. G. de Gennes and C. Taupin, J. Phys. Chem. **86**, 2294 (1982).

[23] K. R. Mecke, Z. Phys. B **97**, 379 (1995).